ACT Publication No. 11-09

Land-cover classification in a moist tropical region of Brazil with Landsat Thematic Mapper imagery

G. Li, D. Lu, E.F. Moran & S. Hetrick

In: International Journal of Remote Sensing, 32:23, 8207-8230

Anthropological Center for Training and Research on Global Environmental Change
Indiana University, Student Building 331, 701 E. Kirkwood Ave., 47405-7100, U.S.A.
Phone: (812) 855-6181, Fax: (812) 855-3000, Email: act@indiana.edu, internet: www.indiana.edu/~act

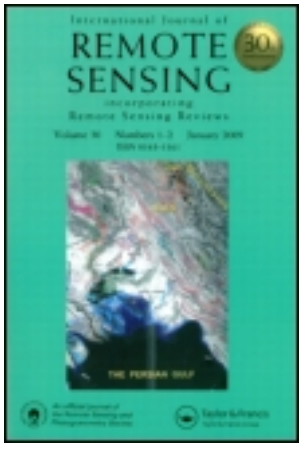

International Journal of Remote Sensing

Publication details, including instructions for authors and subscription information:
http://www.tandfonline.com/loi/tres20

Land-cover classification in a moist tropical region of Brazil with Landsat Thematic Mapper imagery

Guiying Li [a], Dengsheng Lu [a], Emilio Moran [a] & Scott Hetrick [a]

[a] Anthropological Center for Training and Research on Global Environmental Change (ACT), Indiana University, Bloomington, Indiana, 47405, USA

Available online: 09 Aug 2011

To cite this article: Guiying Li, Dengsheng Lu, Emilio Moran & Scott Hetrick (2011): Land-cover classification in a moist tropical region of Brazil with Landsat Thematic Mapper imagery, International Journal of Remote Sensing, 32:23, 8207-8230

To link to this article: http://dx.doi.org/10.1080/01431161.2010.532831

International Journal of Remote Sensing
Vol. 32, No. 23, 10 December 2011, 8207–8230

Taylor & Francis
Taylor & Francis Group

Land-cover classification in a moist tropical region of Brazil with Landsat Thematic Mapper imagery

GUIYING LI*, DENGSHENG LU, EMILIO MORAN and SCOTT HETRICK
Anthropological Center for Training and Research on Global Environmental Change (ACT), Indiana University, Bloomington, Indiana 47405, USA

(*Received 9 July 2010; in final form 23 September 2010*)

This research aims to improve land-cover classification accuracy in a moist tropical region in Brazil by examining the use of different remote-sensing-derived variables and classification algorithms. Different scenarios based on Landsat Thematic Mapper (TM) spectral data and derived vegetation indices and textural images and different classification algorithms, maximum likelihood classification (MLC), artificial neural network (ANN), classification tree analysis (CTA) and object-based classification (OBC), were explored. The results indicate that a combination of vegetation indices as extra bands into Landsat TM multi-spectral bands did not improve the overall classification performance, but the combination of textural images was valuable for improving vegetation classification accuracy. In particular, the combination of both vegetation indices and textural images into TM multi-spectral bands improved the overall classification accuracy (OCA) by 5.6% and the overall kappa coefficient (OKC) by 6.25%. Comparison of the different classification algorithms indicated that CTA and ANN have poor classification performance in this research, but OBC improved primary forest and pasture classification accuracies. This research indicates that use of textural images or use of OBC are especially valuable for improving the vegetation classes such as upland and liana forest classes that have complex stand structures and large patch sizes.

1. Introduction

Since the 1970s, deforestation in the Brazilian Amazon has converted a vast area of primary forest into a mosaic of large patches of agricultural lands, pasture and different stages of successional vegetation (Moran *et al.* 1994a, Skole *et al.* 1994, Lucas *et al.* 2000, Roberts *et al.* 2002, Lu *et al.* 2008). The unprecedented tropical deforestation rates have been regarded as an important factor in climate change and environmental degradation at regional and global scales (Skole *et al.* 1994). In order to better understand the consequences of deforestation and landscape transformations in the region, the timely mapping and monitoring of land-use/cover change is required. Remote-sensing technologies are useful tools in providing these datasets. Much research has been conducted to classify land cover, especially vegetation classes (Mausel *et al.* 1993, Moran *et al.* 1994a,b, Brondízio *et al.* 1996, Foody *et al.* 1996, Rignot *et al.* 1997, Yanasse *et al.* 1997, Lucas *et al.* 2002, Vieira *et al.* 2003, Lu *et al.* 2004a, 2007, 2008, Lu 2005a). Different classification methods, such as traditional

*Corresponding author. Email: ligu@indiana.edu

International Journal of Remote Sensing
ISSN 0143-1161 print/ISSN 1366-5901 online © 2011 Taylor & Francis
http://www.tandf.co.uk/journals
http://dx.doi.org/10.1080/01431161.2010.532831

pixel-based classifiers (e.g. Euclidean distance and maximum likelihood) (Foody *et al.* 1996, Yanasse *et al*. 1997, Vieira *et al.* 2003), a combination of spectral and spatial information (Mausel *et al.* 1993, Moran *et al.* 1994a,b, Lu *et al.* 2004a) and use of sub-pixel information (Roberts *et al.* 1998, Lu *et al.* 2003) have been examined. Castro *et al.* (2003) summarized many approaches using space-borne remotely sensed data to quantify successional forest classification based on biomass or age estimation. Lu (2005a) and Lu *et al.* (2003, 2008) summarized the major methods for mapping vegetation types, especially successional vegetation stages with remotely sensed data in the moist tropical regions of the Brazilian Amazon.

Previous research has indicated that a major source of confusion often occurs in identifying different successional stages or distinguishing between advanced secondary succession and mature forest (Lu *et al*. 2003, 2008), since remotely sensed data primarily capture canopy information, and the canopy structures between advanced secondary succession and mature forest can be very similar, although they may have different ages, species composition and biomass density. The smooth transition between different successional stages also causes problems for vegetation classification. Therefore, previous research often provides only coarse vegetation classes such as primary forest and successional vegetation (Adams *et al.* 1995, Roberts *et al.* 2002). However, the biomass densities of different successional stages vary considerably, ranging from less than 2 kg m^{-2} in initial successional vegetation to greater than 20 kg m^{-2} in advanced successional vegetation (Lu 2005b). The biomass densities of primary forests also vary considerably, ranging from approximately 12 kg m^{-2} to greater than 50 kg m^{-2} in different biophysical environments. Obviously, a single class of primary forest or successional vegetation is not suitable for many applications such as carbon estimations or land degradation assessments.

Remote-sensing image classification is a complex process that involves many steps such as definition of a land-cover classification system, collection of data sources (e.g. reference data, different sensor data), extraction of remote-sensing variables, selection of classification algorithm and accuracy assessment (Jensen 2004, Lu and Weng 2007). Great progress in image classification has been achieved, including: (1) the development of advanced classification algorithms (e.g. neural network, decision tree, support vector machine, object-based algorithms and sub-pixel-based algorithms) (Tso and Mather 2001, Franklin and Wulder 2002, Lu and Weng 2007, Rogan *et al*. 2008, Blaschke 2010), (2) the use of multi-source data in a classification process such as integration of different spatial resolution or sensor images (Solberg *et al.* 1996, Pohl and Van Genderen 1998, Ali *et al*. 2009, Ehlers *et al*. 2010, Zhang 2010) and the integration of remote sensing and ancillary data (Harris and Ventura 1995, Williams 2001, Li 2010) and (3) the development of techniques for modifying classified images by the use of expert knowledge (Stefanov *et al.* 2001, Hodgson *et al*. 2003, Zhang *et al*. 2011).

In practice, Landsat Thematic Mapper (TM) images are still the most common data source for land-cover classification, even in moist tropical regions, due to their suitable spectral and spatial resolutions and the long-term data availability since the 1970s. Although much research related to land-cover classification has been conducted, a comprehensive analysis of the selection of variables and classification algorithms has not been fully investigated. Therefore, this research aims to explore how combinations of different variables can improve land-cover classification performance and which classification algorithm has better classification performance in the moist tropical region of Brazil. This research investigates the roles of vegetation indices and textural images in improving vegetation classification performance based on a comparison of

accuracy assessment of the classified images and compares parametric and nonparametric algorithms in order to understand which classification algorithm is suitable for vegetation classification in the moist tropical region of the Brazilian Amazon, where complex forest stand structure in successional vegetation and primary forest exists. Through this research, we can better understand the classification procedure, including the selection of suitable remote-sensing variables and the selection of classification algorithms, for the vegetation classification in the Brazilian Amazon.

2. Study area

Altamira is located along the Transamazon Highway (BR-230) in the northern Brazilian state of Pará. The city of Altamira lies on the Xingu River at the eastern edge of the study area (see figure 1). In the 1950s, an effort was made to attract colonists from throughout Brazil, who came and settled along streams as far as 20 km from the city centre. With the construction of the Transamazon Highway in 1970, this population and older caboclo settlers from earlier rubber boom eras claimed land along the new highway and legalized their land claims. Early settlement was driven by geopolitical goals of settling the north region of Brazil and political economic policies aimed to shift production of staples like rice, corn and beans from the most southern Brazilian states to the northern region. The uplands are somewhat rolling, with a highest elevation of approximately 350 m. Floodplains along the Xingu are flat with a lowest elevation of approximately 10 m. The nutrient-rich Alfisols and infertile Ultisols and Oxisols are found in the uplands of this area. The overall soil quality of this area is above average fertility for Amazonia. The dominant native types of vegetation are mature moist forest and liana forest. Major deforestation began in the area in 1972, coincident with the construction of the Transamazon

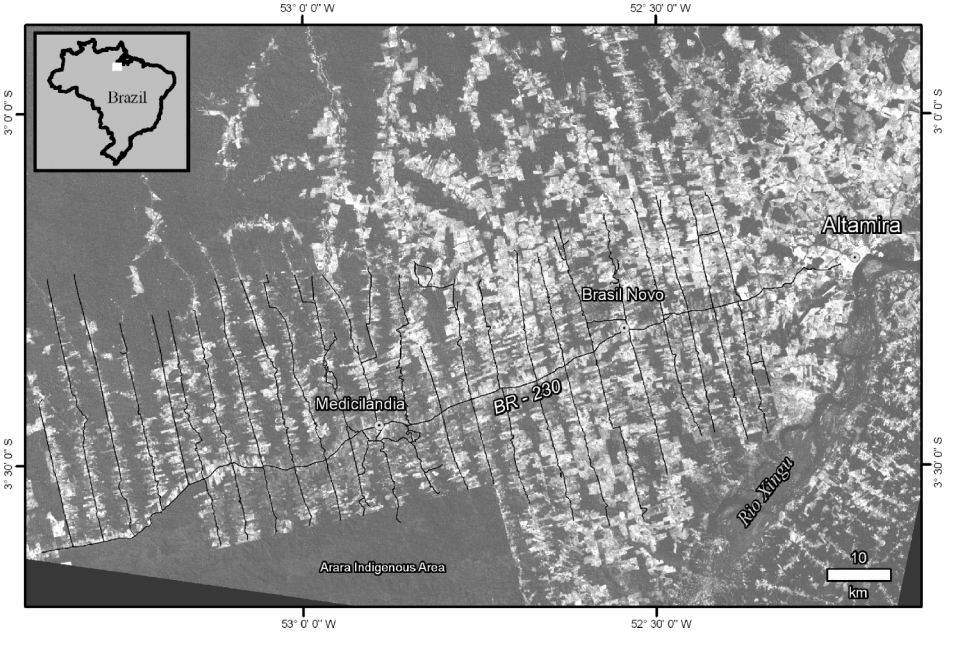

Figure 1. Study area: Altamira, Pará State, Brazil, by overlaying fish-bone roads.

Highway (Moran 1981). Deforestation has led to a complex composition of different vegetation types such as different succession stages and pasture (Moran *et al.* 1994a,b, Moran and Brondízio 1998). Annual rainfall in Altamira is approximately 2000 mm and is concentrated from late October through to early June; the dry period occurs between June and September. The average temperature is about 26°C (Tucker *et al.* 1998).

3. Methods

3.1 *Data collection, organization and preprocessing*

3.1.1 Field data collection and determination of a land-cover classification system. Sample plots for different land covers, especially for different stages of secondary succession and pasture were collected during the summer of 2009 in the Altamira study area. Prior to the fieldwork, candidate sample locations of complex vegetation areas were identified in the laboratory through visual interpretation of a Landsat 5 TM image acquired in July 2008. As shown in figure 1, primary forest is distributed away from the roads, and different stages of succession vegetation, pastures and agricultural lands were distributed along the main and secondary roads, forming the familiar 'fishbone' pattern of deforestation. Because of the difficulty in accessing forested sites in moist tropical regions like this study area, random allocation of sample plots for a field survey is not feasible. Therefore, the majority of sample plots relevant to non-forest vegetation and pastures were allocated along the roadsides. In each sample area, the locations of different vegetation cover types were recorded using a global positioning system (GPS) device, while detailed descriptions of vegetation stand structure (e.g. height, canopy cover, dominant tree species) were recorded. Sketch map forms were used in conjunction with small field maps showing the candidate sample locations on A4 paper to note the spatial extent and patch shape of vegetation cover types in the area surrounding the GPS point. Following fieldwork, GPS points and field survey data were organized and stored in a data base. Geographic information systems (GISs) and remote-sensing software were used to create representative regions of interest (ROI). ROIs were created by identifying areas of uniform pixel reflectance in an approximate 3×3 pixel window size on the Landsat TM imagery. Approximately half of the samples from the field survey were used for training samples for image classification, and the rest were used as test samples for accuracy assessment. Meanwhile, a QuickBird image acquired in September 2008 was also used to support the selection of more sample plots for use as training and test sample plots. According to the research objectives, compatibility with previous research work (Mausel *et al.* 1993, Moran *et al.* 1994a,b, Moran and Brondízio 1998) and field surveys, the land-cover classification system including three forest classes (i.e. upland (UPF), flooding (FLF) and liana (LIF)), three succession stages (i.e. initial (SS1), intermediate (SS2) and advanced (SS3)), pasture (PAS) and four non-vegetated classes (i.e. water (WAT), wetland (NVW), urban (URB) and burn scars (BUR)), were designed and used for this research.

3.1.2 Image collection and preprocessing. A Landsat 5 TM image acquired on 2 July 2008 was geometrically registered to a previously corrected Landsat 5 TM image with UTM coordinates (zone 22). The geometric error was less than 0.5 pixels. During

image-to-image registration, a nearest-neighbour resampling algorithm was used to resample the TM imagery in order to avoid a change of digital numbers and keep the same pixel size of 30 × 30 m as the original image. An improved image-based dark object subtraction (DOS) model was used to perform radiometric and atmospheric correction (Chavez 1996, Lu *et al*. 2002, Chander *et al.* 2009). The gain and offset for each band and sun elevation angle were obtained from the image header file. The path radiance for each band was identified from deep-water bodies. The geometrically corrected and atmospherically calibrated TM image was used to develop vegetation indices and textural images.

3.2 *Selection of remote-sensing variables for land-cover classification*

Since the vegetation classification is especially important in this research, the objective of selecting vegetation indices and textural images is to enhance the separability of vegetation types, especially for different primary forest classes and secondary succession (SS) stages. Therefore, training samples for three forest types (UPF, FLF and LIF), three succession stages (SS1, SS2 and SS3) and pasture were selected for evaluating the separability of vegetation types in order to identify suitable vegetation indices and textural images for improving vegetation classification accuracies.

3.2.1 Selection of vegetation indices. Many vegetation indices have been used for different purposes such as estimation of biophysical parameters (Bannari *et al.* 1995, McDonald *et al.* 1998). Lu *et al.* (2004b) examined the relationships between vegetation indices and forest stand structure attributes such as aboveground biomass (AGB), average stand diameter and height in different biophysical conditions in the Brazilian Amazon. They found that vegetation indices containing TM band 5 had higher correlation coefficients with forest stand parameters (e.g. AGB) than those without band 5 such as the normalized difference vegetation index (NDVI) in Altamira, where forest stand structure is very complex, while NDVI had a higher correlation with forest stand parameters in Bragantina, where forest stand structure is much simpler. This is because the complex forest stand structures result in higher spectral variation in near-infrared wavelengths (TM band 4) within the forest class or the successional vegetation than those simple stand structures. Therefore, in this research, different vegetation indices including band 5 were designed, together with the other indices summarized in table 1.

In order to identify suitable vegetation indices for improving vegetation classification performance, training sample plots for different vegetation types were selected from field surveys for conducting separability analysis with the transformed divergence (TD) algorithm (Mausel *et al.* 1990, Landgrebe 2003). Individual vegetation indices and combinations of two or more vegetation indices were investigated. When different combinations of two or more indices were tested, Lu *et al.* (2008) proposed to identify the best combination based on TD values and correlation coefficients. However, some combinations of vegetation indices have similar TD values, thus this method cannot determine the best combination for vegetation classification. In general, a higher standard deviation value of an image indicates higher information load, implying better performance for land-cover classification. Therefore, this research modified the previously used method by replacing TD with standard deviation. When the potential combination of vegetation index images are selected on the basis of TD analysis,

Table 1. Vegetation indices used in the research.

No.	Vegetation index	Equation
1	TC1	0.304TM1+0.279TM2+0.474TM3+0.559TM4+0.508TM5+0.186TM7
2	TC2	−0.285TM1−0.244TM2−0.544TM3+0.704TM4+0.084TM5−0.180TM7
3	TC3	0.151TM1+0.197TM2+0.328TM3+0.341TM4−0.711TM5−0.457TM7
4	ASVI	$((2\mathrm{NIR}+1)-\sqrt{(2\mathrm{NIR}+1)^2-8(\mathrm{NIR}-2\mathrm{RED}+\mathrm{BLUE})})/2$
5	MSAVI	$((2\mathrm{NIR}+1)-\sqrt{(2\mathrm{NIR}+1)^2-8(\mathrm{NIR}-2\mathrm{RED})})/2$
6	ND4-2	(TM4−TM2)/(TM4+TM2)
7	ND4-25	(TM4−TM2−TM5)/(TM4+TM2+TM5)
8	ND42-53	(TM4+TM2−TM5−TM3)/(TM4+TM2+TM5+TM3)
9	ND42-57	(TM4+TM2−TM5−TM7)/(TM4+TM2+TM5+TM7)
10	ND4-35	(TM4−TM3−TM5)/(TM4+TM3+TM5)
11	ND45-23	(TM4+TM5−TM2−TM3)/(TM4+TM5+TM2+TM3)
12	ND4-57	(2TM4−TM5−TM7)/(TM4+TM5+TM7)
13	NDVI	(TM4−TM3)/(TM4+TM3)
14	NDWI	(TM4-TM5)/(TM4+TM5)

Note: ND, normalized difference; ASVI, atmospheric and soil vegetation index; MSAVI, modified soil adjusted vegetation index; NDVI, normalized difference vegetation index; NDWI, normalized difference water index; TC, tasselled cap transform.

the best combination (C) is determined from the analysis of standard deviation and correlation coefficients according to equation (1):

$$C = \sum_{i=1}^{n} S_i \Big/ \left| \sum_{j=1}^{n} R_{ij} \right|, \tag{1}$$

where S_i is the standard deviation of the vegetation index image i, R_{ij} is the correlation coefficient between two vegetation index images i and j and n is the number of vegetation index images. A higher C value indicates a better combination of vegetation indices for vegetation classification.

3.2.2 Selection of textural images. Many texture measures have been developed and proper use of textural images has proven useful in improving land-cover classification accuracy (Haralick *et al.* 1973, Kashyap *et al.* 1982, Marceau *et al.* 1990, Augusteijn *et al.* 1995, Shaban and Dikshit 2001, Chen *et al.* 2004, Lu *et al.* 2008). Of the many texture measures, grey level co-occurrence matrix (GLCM)-based textural images have been extensively used for land-cover classification (Marceau *et al.* 1990, Lu *et al.* 2008). Lu (2005b) has explored the roles of textural images in AGB estimation and found that textural image based on variance with TM band 2 and a window size of 9 × 9 pixels had a significant relationship with AGB. In another study, Lu *et al.* explored textural images in vegetation classification and found that textural images based on entropy, second moment, dissimilarity and contrast with window sizes of 7 × 7 or 9 × 9 pixels had a better performance in Rondonia State (Lu *et al.* 2008). Therefore, in this research, GLCM-based texture measures, variance, homogeneity, contrast, dissimilarity and entropy (see table 2 for their formulas) were employed with a window size of 9 × 9 pixels and Landsat TM bands 2, 3, 4, 5 and 7. Separability analysis with a TD based on selected training sample plots of different vegetation classes was used for the selection of a potential single textural image and a combination of two or more

Table 2. Texture measures used in the research.

No.	Texture measures	Formula
1	Variance (VAR)	$\mathrm{VAR} = \sum_{i,j=0}^{N-1} P_{i,j}(i - \mathrm{ME})^2$
2	Homogeneity (HOM)	$\mathrm{HOM} = \sum_{i,j=0}^{N-1} \frac{P_{i,j}}{1+(i-j)^2}$
3	Contrast (CON)	$\mathrm{CON} = \sum_{i,j=0}^{N-1} P_{i,j}(i-j)^2$
4	Dissimilarity (DIS)	$\mathrm{DIS} = \sum_{i,j=0}^{N-1} P_{i,j}\lvert i-j\rvert$
5	Entropy (ENT)	$\mathrm{ENT} = \sum_{i,j=0}^{N-1} P_{i,j}(-\ln P_{i,j})$

Note: $P_{i,j} = V_{i,j} / \sum_{i,j=0}^{N-1} V_{i,j}$, $\mathrm{ME} = \sum_{i,j=0}^{N-1} i(P_{i,j})$, where $V_{i,j}$ is the value in cell i, j (row i and column j) of the moving window and N is the number of rows or columns.

textural images. When two or more textural images were selected, correlation coefficients between textural images and the standard deviation of each textural image were used to identify the C according to equation (1).

3.3 *Land-cover classification*

Four classification algorithms, maximum likelihood classification (MLC), artificial neural network (ANN), classification tree analysis (CTA) and object-based classification (OBC) were selected in this research. In order to identify a suitable classification algorithm, the classification results from the four algorithms based on original TM six spectral bands and the C of spectral bands, vegetation indices and textural images were analysed, for which the same training and test samples were used. A total of 254 sample plots (over 3500 pixels) covering the 11 land covers, where each land cover had 15–30 plots, were used for each classification algorithm.

3.3.1 Maximum likelihood classification (MLC). MLC is the most common parametric classifier that assumes normal or near-normal spectral distribution for each feature of interest and an equal prior probability among the classes. This classifier is based on the probability that a pixel belongs to a particular class. It takes the variability of classes into account by using the covariance matrix. A detailed description of MLC can be found in many textbooks (e.g. Richards and Jia 1999, Lillesand and Kiefer 2000, Jensen 2004). In this research, MLC was used to conduct land-cover classification based on different scenarios in order to explore the roles of vegetation indices and textural images in improving land cover, especially vegetation classification in the moist tropical region. The scenarios included: (1) TM six spectral bands, (2) selected vegetation indices, (3) selected textural images, (4) combination of selected vegetation indices and textural images, (5) combination of spectral bands and vegetation indices, (6) combination of spectral bands and textural images and (7) combination of spectral bands, vegetation indices and textural images. These classification results were evaluated with accuracy assessment methods. The best scenario was further analysed with

nonparametric classification algorithms, as well as the TM spectral bands for the sake of comparison.

3.3.2 Artificial neural networks (ANNs). ANNs have gained great interest as a classification technique during past decades (Bischof *et al.* 1992, Paola and Schowengerdt 1995, Bruzzone *et al.* 1997, Kanellopoulos and Wilkinson 1997) because no assumptions about a feature's distribution (distribution free) and no *a priori* knowledge about the statistical characteristics of feature class data are required. Of the different neural-network models, the multi-layer perceptron (MLP) trained by a back propagation (BP) algorithm is one of the most widely used models (Kanellopoulos and Wilkinson 1997, Tso and Mather 2001). Typically, an MLP consists of one input layer, one output layer and one or more hidden layers. Each layer contains neurons, and each neuron is connected to every neuron in the adjacent layers by a weighted connection. In general, a single hidden layer MLP is approximate for most classification problems. The number of neurons in the input layer and output layer are determined by the number of layers of images used for classification and the number of categories in classification results, respectively. However, the number of neurons in hidden layers is not straightforward to define. It requires lengthy experiments in combining with other parameters such as learning rate, number of iterations and momentum factor to produce the best results. In this research, MLP was conducted using a sigmoid activation function.

3.3.3 Classification tree analysis (CTA). CTA is a nonparametric statistical machine learning algorithm, having such advantages as distribution free and easy interpretation over traditional supervised classifiers, and thus has received increasing attention in remote-sensing classification (Hansen *et al*. 1996, Friedl and Brodley 1997, Zambon *et al*. 2006). The basic concept of a classification tree is to split a dataset into homogeneous subgroups based on measured attributes. The tree is composed of a root node, representing variables or attributes, a set of internal nodes (branches), representing attribute values used to split, and a set of terminal nodes (leaves), representing classes. Each node makes a binary decision that separates either one class or some of the classes from the remaining classes. The processing starts at the root and follows the branches until the leaf node is reached. This is known as a top-down approach. Different splitting rules were used in previous studies (Zambon *et al*. 2006). In this research, three types of splitting rules, ratio, entropy and Gini, were examined. The training samples were used to grow classification trees, and the whole image was then classified with them. Based on experimentation, the ratio-splitting method was selected for this research.

3.3.4 Object-based classification (OBC). Per-pixel-based classification algorithms often result in a salt-and-pepper effect in the classified image. In order to reduce this problem, different techniques have been used, including image processing (e.g. low-pass filter, texture analysis) (Gong 1994, Hill and Foody 1994), contextual classification (Gong and Howarth 1992) and post-classification processing (e.g. mode filtering, morphological filtering, rule-based processing and probabilistic relaxation) (Shackelford and Davis 2003, Sun *et al*. 2003). OBC provides a useful alternative compared to the traditional per-pixel methods because it classifies a remotely sensed image based on image segments. Segmentation is the process partitioning images into

isolated objects so that each object shares a homogeneous spectral similarity. These objects better represent the landscape than the original pixels do. The homogeneous objects are then analysed using traditional classification methods such as minimum distance and MLC (Jensen 2004, Lu *et al*. 2010). Different image-segmentation algorithms, such as Split and Merge, Watershed, K-means, Finite Gaussian Mixture and Markov Random Field, have been developed (Yu *et al*. 2006, Blaschke 2010). The Watershed delineation approach was used in this study. The classification process consists of three steps: (1) image segmentation, a moving window assesses spectral similarity across space and over all input bands, and segments are defined based on user-specified similarity thresholds, (2) creation of training sites and signature classes based on image segments and (3) classification of the segments. This is carried out with the assistance of a reference image, which is an already classified image and which is used to assign the majority class within each segment. Training sites (polygons), which coincide with the sample sites used in MLC, ANN and CTA, were selected on the segmented image. The classified image from MLC was used as a reference image.

3.4 *Accuracy assessment*

A common method for accuracy assessment is through the use of an error matrix. An error matrix can provide a detailed assessment of the agreement between the classified result and reference data and provide information of how the misclassification happened (Congalton and Green 2008). In addition, different accuracy assessment parameters, such as overall classification accuracy (OCA), producer's accuracy (PA), user's accuracy (UA) and overall kappa coefficient (OKC), can be calculated from the error matrix, as previous literature has described (e.g. Congalton 1991, Smits *et al.* 1999, Foody 2002, 2004, Wulder *et al.* 2006, Congalton and Green 2008, Foody 2009). OCA considers only the total number of correctly classified class without taking into account the omission and commission errors, thus it does not reveal whether errors were evenly distributed between classes or whether some classes were really bad and some really good. The OKC is a measure of overall statistical agreement of an error matrix, which takes non-diagonal elements into account. Kappa analysis is recognized as a powerful method for analysing a single error matrix and for comparing the differences between various error matrices (Congalton 1991, Smits *et al.* 1999, Foody 2002, 2004). Both OCA and OKC reflect the overall classification situation, which cannot provide the reliability of some land-cover classes of interest; thus, PA and UA for each land-cover class are often used to provide a complementary analysis of the accuracy assessment. In this study, a total of 338 test sample plots from the field survey and the QuickBird image were used for accuracy assessment. An error matrix was developed for each classified image and then PA and UA for each class and OCA and OKC for each classified image were calculated from the corresponding error matrix.

4. Results

4.1 *Identification of vegetation indices and textural images*

The separabiltiy analysis based on training samples indicated that the single vegetation index such as ND4-25, TC2, ND42-53, ND4-35 and TC3 and the single textural images from the dissimilarity on TM band 2 or band 3 (TM2-DIS, TM3-DIS), contrast on TM band 2 (TM2-CON) and homogeneity on TM band 2 or band 3

Table 3. Summary of potential vegetation indices and textural images.

		Potential bands	Best band
Vegetation indices	Single	ND4-25, TC2, ND42-53, ND4-35 and TC3	
	Combination	TC2 with any of the following: TC3, ND42-53, ND42-57, ND4-57, ND4-35, NDWI, ND42-53, ND4-25; ND42-57 with ND4-2, ND4-25, ND42-53, ND4-35 and NDWI; TC1 with TC3, ND4-25, ND42-53, ND42-57, ND4-37 and NDWI.	TC2 and ND42-57
Textural images	Single	TM2 or TM3-DIS, TM2-CON, TM2 or TM3-HOM	
	Combination	TM2-DIS with all texture measures based on bands TM3, 4, 5 and 7; TM2-HOM with TM4-CON or DIS, TM7-CON or DIS; TM2-CON with TM4-CON or DIS, TM7-CON or DIS; TM3-DIS with TM4, TM5 and TM7- HOM, CON and DIS	TM2-DIS and TM4-DIS

Note: The formulas for vegetation indices and texture measures are summarized in tables 1 and 2.

(TM2-HOM or TM3-HOM) (see table 3) have relatively high TD values, but no single vegetation index or textural image can successfully separate these vegetation types. According to the separability analysis and the *C* value, a combination of two vegetation indices or two textural images provided the best results for vegetation separability. The combination of three or more vegetation indices or textural images did not significantly improve the vegetation separability, a similar conclusion to our previous research (Lu *et al.* 2008). According to the analysis of the *C* value, the *C* for two vegetation indices was TC2 and ND42-57 and the *C* for two textural images was TM2-DIS and TM4-DIS (dissimilarity based on TM band 2 and band 4). Figure 2 provides a comparison of TM spectral bands, two selected vegetation indices and textural images, showing the different features for vegetation types, especially between spectral bands and textural images.

4.2 *Accuracy assessment of land-cover classification images based on MLC and analysis of the roles of vegetation indices and textural images in improving land-cover classification accuracy*

The accuracy assessment result from Landsat TM six spectral bands with MLC (see table 4) indicated that the major errors were due to the confusions of vegetation types such as among the three forest classes (i.e. UPF, FLF and LIF) and among SS2, SS3, LIF and UPF. URB is also confused with WAT and NVW because URB is often a complex landscape and dark impervious surfaces in urban landscape have similar spectral signatures with WAT and/or NVW. Although the TD analysis indicated that the selected combination of two vegetation indices or two textural images was optimal for vegetation separation based on training sample plots, the accuracy assessment showed that their overall accuracies (i.e. OCA and OKC) were much lower than from the classification results based on six spectral bands (see table 5). However, the classification accuracy showed that the combination of vegetation indices and textural images improved classification performance, with similar OCA as the TM six spectral

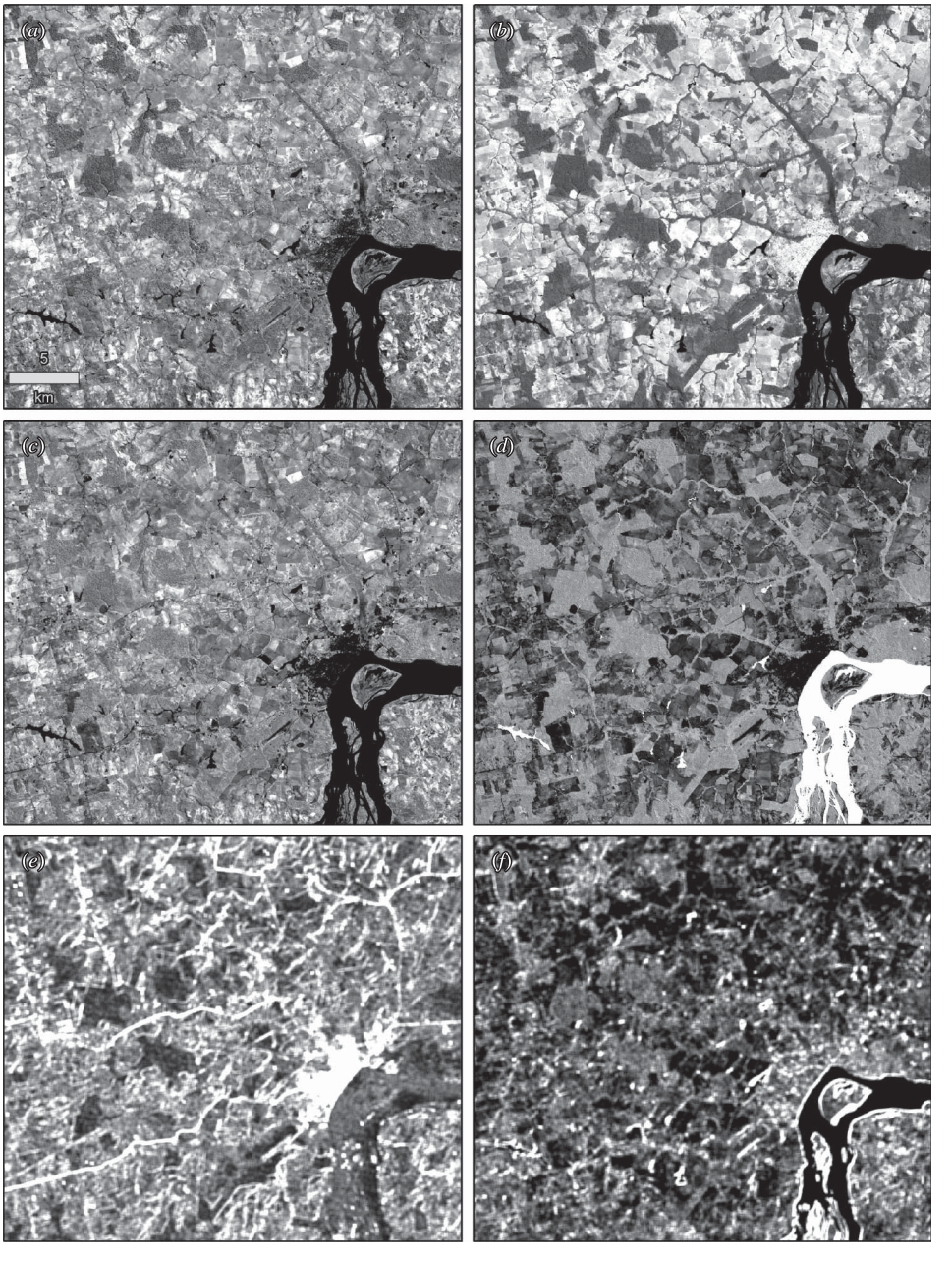

Figure 2. A comparison of TM band 4, band 5, two vegetation indices and two textural images. (*a*), (*b*) TM bands 4 and 5; (*c*), (*d*) the second component from tasselled cap transformation and the vegetation index based on bands 4, 2, 5 and 7; (*e*), (*f*) textural images based on dissimilarity on band 2 and band 4 and window size of 9 × 9 pixels.

bands. In particular, this combination improved classification performance for forest classes, that is, UPF, FLF and LIF.

The combination of vegetation indices as extra bands into TM multi-spectral bands had a limited role in improving overall classification performance, but was helpful in

Table 4. Error matrix from MLC based on the Landsat TM six spectral bands.

	UPF	FLF	LIF	SS1	SS2	SS3	PAS	WAT	NVW	URB	BUR	RT	CT	PA	UA
UPF	20	1	0	0	0	0	0	0	0	0	0	21	54	37.0	95.2
FLF	15	15	0	0	0	0	0	0	0	0	0	30	16	93.8	50.0
LIF	13	0	42	0	4	3	0	0	1	0	0	63	44	95.5	66.7
SS1	1	0	0	21	1	0	11	0	0	0	0	34	25	84.0	61.8
SS2	0	0	0	2	19	0	0	0	0	0	0	21	28	67.9	90.5
SS3	5	0	0	0	4	26	0	0	0	0	0	35	29	89.7	74.3
PAS	0	0	0	2	0	0	55	0	1	0	0	58	66	83.3	94.8
WAT	0	0	0	0	0	0	0	15	0	0	0	15	22	68.2	100
NVW	0	0	0	0	0	0	0	0	7	0	0	7	13	53.9	100
URB	0	0	0	0	0	0	0	7	4	27	0	38	27	100	71.1
BUR	0	0	2	0	0	0	0	0	0	0	14	16	14	100	87.5
OCA = 77.2%, OKC = 0.745															

Note: RT and CT represent row total and column total; UA and PA represent user's accuracy (%) and producer's accuracy (%); OCA and OKC represent overall classification accuracy (%) and overall kappa coefficient.

Table 5. Comparison of accuracy assessment results among different scenarios based on MLC.

	6SB		2VI		2TX		2VI&2TX		6SB&2VI		6SB&2TX		6SB&2VI&2TX	
Land cover	PA	UA	PA	UA	PA	UA	PA	UA	PA	UA	PA	UA	PA	UA
UPF	37.0	95.2	18.5	66.7	61.1	61.1	66.7	75.0	24.2	92.9	66.7	78.3	66.7	78.3
FLF	93.8	50.0	100	37.2	0.0	0.0	100	72.7	100	41.0	100	66.7	100	69.6
LIF	95.5	66.7	95.5	59.2	77.3	30.6	86.4	67.9	95.5	63.6	81.8	66.7	84.1	69.8
SS1	84.0	61.8	64.0	48.5	36.0	34.6	92.0	52.3	80.0	64.5	92.0	57.5	92.0	59.0
SS2	67.9	90.5	46.4	65.0	3.6	14.3	50.0	82.4	67.9	86.4	78.6	95.7	82.1	92.0
SS3	89.7	74.3	82.8	75.0	0	0	72.4	65.6	86.2	75.8	79.3	85.2	86.2	89.3
PAS	83.3	94.8	75.8	86.2	54.6	51.4	69.7	95.8	86.4	95.0	75.8	96.2	77.3	98.1
WAT	68.2	100	100	100	50.0	73.3	100	100	95.5	100	72.7	100	95.5	100
NVW	53.9	100	38.5	100	0.0	0.0	38.5	83.3	69.2	90.0	69.2	100	53.9	87.5
URB	100	71.1	92.6	96.2	100	81.8	100	96.4	100	100	100	79.4	100	100
BUR	100	87.5	78.6	84.6	28.6	21.1	85.7	80.0	92.9	86.7	92.9	100	100	87.5
OCA	77.2		69.2		45.9		76.9		77.5		80.2		82.8	
OKC	0.745		0.656		0.378		0.741		0.749		0.777		0.807	

Note: SB, VI and TX represent TM multi-spectral bands, vegetation indices and textural images; UA and PA represent user's accuracy (%) and producer's accuracy (%); OCA and OKC represent overall classification accuracy (%) and overall kappa coefficient.

improving the separability of PAS, WAT and URB from other land covers; in contrast, the combination of textural images into spectral bands was valuable for improving vegetation classification accuracy, especially for UPF, FLF, SS2 and SS3 and improved OCA by 3%, as indicated in table 5. The high correlation between vegetation indices and spectral bands, as shown in table 6, limited the role of vegetation indices in improving vegetation classification accuracy. The second component (TC2) from the tasselled cap (TC) transform mainly represented the vegetation information, as indicated in the constants in the TC transform (see table 1), which had very high correlation with the near-infrared band (0.83), while the ND42-57 image had a strongly negative correlation with visible bands (bands 1–3) and shortwave infrared bands (bands 5 and 7), which mainly reflected the overall brightness, good for separation of non-vegetation classes. In contrast, textural images, either based on TM band 2 or band 4, had relatively low correlation with spectral signatures, thus, incorporation of textural images improved land-cover classification performance.

The combination of both vegetation indices and textural images with multi-spectral bands provided the best classification performance, with OCA and OKC increased by 5.6% and 6.2%, respectively, compared with the result from MLC on the TM multi-spectral bands (see table 5). However, even in this best scenario, that is, the combination of vegetation indices and textural images into multi-spectral bands, high confusion still existed between UPF, FLF and LIF among different successional stages and between SS2, SS3 and forest classes (see table 7). Figure 3 provides a comparison of classification results among the four scenarios. It indicates that use of textural images (see figure 3(*c*) and (*d*)) reduced the salt-and-pepper effect in the classified image, which is often a problem with per-pixel-based classification methods. This research implies that use of textural images can reduce the heterogeneity of forest stand structure, thus improving the vegetation classification accuracies.

4.3 *Analysis of land-cover classification results among different classification algorithms*

The comparison of accuracy assessment results among different classification algorithms (see table 8) indicates that the OBC and MLC outperformed CTA and MLP for both datasets. In particular, OBC provided the best classification accuracy and the MLP provided the poorest accuracy. Table 8 indicates that the OBC was especially valuable for the forest classes (i.e. UPF, FLF and LIF) and pasture whose patch size was relatively large; in contrast, this method did not improve the classification performance of secondary succession (SS) stages (i.e. SS1, SS2, SS3) because of their relatively small patch size. Table 8 also indicates the importance of using both the vegetation indices and textural images in improving land-cover classification performance, no matter what classification algorithms were used. Figure 4 shows part of the classified images based on these four classification algorithms from the combination of spectral bands, vegetation indices and textural images. Visual interpretation of the classified images by comparing with the TM colour composite indicates that the CTA overestimated forest but underestimated SS, while MLP obviously underestimated SS classes.

5. Discussion

5.1 *Selection of suitable variables for land-cover classification*

Much previous research has shown the importance of using textural images in improving land-cover classification accuracies (Kurosu *et al.* 2001, Shaban and Dikshit 2001,

Table 6. Correlation coefficients between selected images.

	B1	B2	B3	B4	B5	B7	TC2	ND42-57	B2-DIS	B4-DIS
B1	1.00	0.91	0.91	0.41	0.85	0.86	−0.14	−0.71	0.51	−0.21
B2	0.91	1.00	0.94	0.52	0.91	0.88	−0.03	−0.68	0.54	−0.27
B3	0.91	0.94	1.00	0.33	0.88	0.89	−0.25	−0.78	0.55	−0.24
B4	0.41	0.52	0.33	1.00	0.60	0.38	0.83	−0.01	0.21	−0.24
B5	0.85	0.91	0.88	0.60	1.00	0.96	0.09	−0.78	0.48	−0.33
B7	0.86	0.88	0.89	0.38	0.96	1.00	−0.16	−0.90	0.50	−0.28
TC2	−0.14	−0.03	−0.25	0.83	0.09	−0.16	1.00	0.47	−0.11	−0.11
ND42-57	−0.71	−0.68	−0.78	−0.01	−0.78	−0.90	0.47	1.00	−0.44	0.22
B2-DIS	0.51	0.54	0.55	0.21	0.48	0.50	−0.11	−0.44	1.00	0.17
B4-DIS	−0.21	−0.27	−0.24	−0.24	−0.33	−0.28	−0.11	0.22	0.17	1.00

Note: B1–B7 represent TM bands from 1 to 7, except 6 for the thermal band; TC2 and ND42-57 represent two vegetation indices; B2-DIS and B4-DIS represent two textural images.

Table 7. Error matrix from the MLC on the combination of spectral signature, vegetation indices and textural images.

	UPF	FLF	LIF	SS1	SS2	SS3	PAS	WAT	NVW	URB	BUR	RT	CT	PA	UA
UPF	36	0	5	0	0	3	0	0	2	0	0	46	54	66.7	78.3
FLF	5	16	2	0	0	0	0	0	0	0	0	23	16	100	69.6
LIF	11	0	37	0	3	1	0	0	1	0	0	53	44	84.1	69.8
SS1	1	0	0	23	0	0	15	0	0	0	0	39	25	92.0	59.0
SS2	0	0	0	2	23	0	0	0	0	0	0	25	28	82.1	92.0
SS3	1	0	0	0	2	25	0	0	0	0	0	28	29	86.2	89.3
PAS	0	0	0	0	0	0	51	0	1	0	0	52	66	77.3	98.1
WAT	0	0	0	0	0	0	0	21	0	0	0	21	22	95.5	100
NVW	0	0	0	0	0	0	0	1	7	0	0	8	13	53.9	87.5
URB	0	0	0	0	0	0	0	0	0	27	0	27	27	100	100
BUR	0	0	0	0	0	0	0	0	2	0	14	16	14	100	87.5

Note: CT and RT represent column and row total; PA and UA represent producer's and user's accuracy (%).

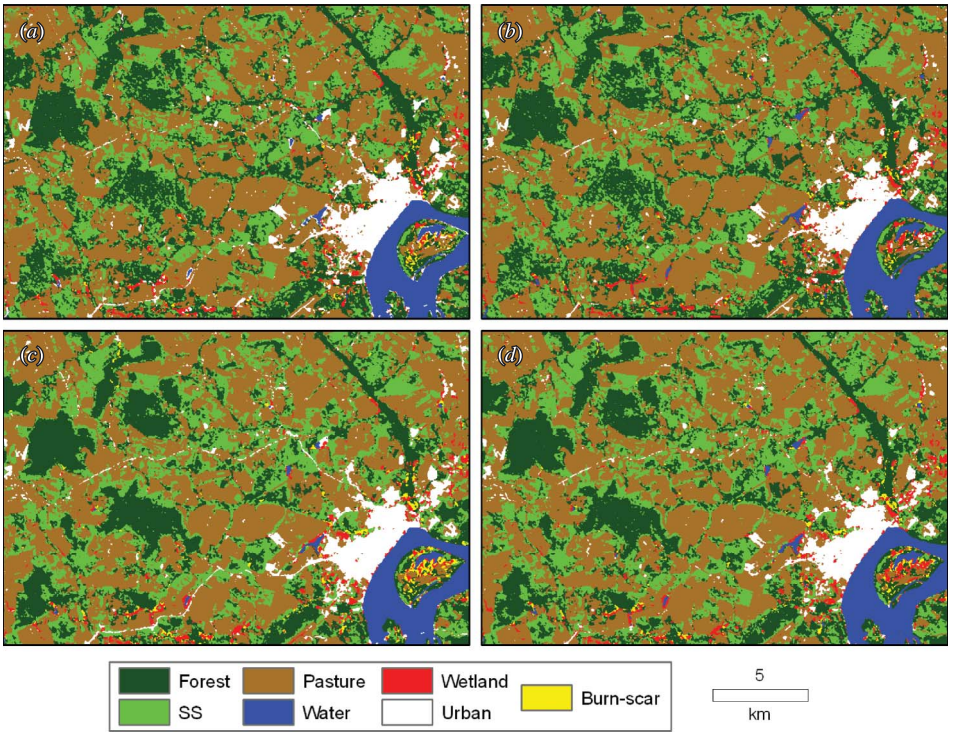

Figure 3. Comparison of classification results among different scenarios with maximum likelihood classifier: (*a*) six TM spectral bands, (*b*) combination of spectral bands and two vegetation indices, (*c*) combination of spectral bands and two textural images and (*d*) combination of spectral bands, two vegetation indices and two textural images. (In order to clearly show the land-cover distribution, three forest classes and three SS classes were merged as forest and SS in this figure.)

Narasimha Rao *et al.* 2002, Podest and Saatchi 2002, Butusov 2003, Lu *et al.* 2008). This research confirms the value of using textural images from Landsat TM data for improving vegetation classification performance in moist tropical regions. One critical step in a study is to identify suitable textural images that can provide the best separability for the specific classes. Selection of suitable textural images can be challenging because textures vary with the characteristics of the landscape under investigation and images used. In particular, the selection of a suitable size of moving window is important for the creation of a textural image, but no window size is perfect for all vegetation types because the patch sizes of the vegetation types can vary greatly, from less than 1 ha for some successional vegetation to hundreds of hectares for primary forests. Therefore, there are tradeoffs among moving window size, spatial resolution of images and the patch sizes of vegetation types of interest on the ground. For the selection of a single textural image, one can select a best textural image based on the highest separability value with the separability analysis, but for the selection of two or more textural images, the *C* approach provides an easy method to identify the suitable combination of textural images that can be used for improving classification performance.

Table 8. Comparison of accuracy assessment results among different classification methods based on the Landsat six spectral bands and based on the combination of the six spectral bands, two vegetation indices and two textural images.

	Data: TM six spectral bands							
	MLC		CTA		MLP		OBC	
Land cover	PA	UA	PA	UA	PA	UA	PA	UA
UPF	37.0	95.2	88.9	58.5	98.2	34.0	53.7	78.4
FLF	93.8	50.0	56.3	75.0	0.0	0.0	93.8	75.0
LIF	95.5	66.7	43.2	34.6	6.8	21.4	95.5	68.9
SS1	84.0	61.8	76.0	59.4	0.0	0.0	72.0	58.1
SS2	67.9	90.5	71.4	87.0	0.0	0.0	67.9	82.6
SS3	89.7	74.3	6.9	100.0	0.0	0.0	72.4	63.6
PAS	83.3	94.8	81.8	94.7	83.3	54.5	81.8	91.5
WAT	68.2	100.0	81.8	100.0	100.0	100.0	77.3	100.0
NVW	53.9	100.0	84.6	68.8	69.2	100.0	53.9	100.0
URB	100.0	71.1	96.3	100.0	96.3	100.0	100.0	77.1
BUR	100.0	87.5	92.9	86.7	57.1	80.0	100.0	93.3
OCA	77.2		70.7		52.1		77.8	
OKC	0.745		0.667		0.436		0.750	
	Data: six spectral bands, two VIs and two textural images							
	MLC		CTA		MLP		OBC	
Land cover	PA	UA	PA	UA	PA	UA	PA	UA
UPF	66.7	78.1	68.5	67.3	90.7	50.0	74.1	85.1
FLF	100.0	69.6	81.3	65.0	81.3	68.4	100.0	72.7
LIF	84.1	69.8	77.3	54.8	45.5	64.5	88.6	75.0
SS1	92.0	59.0	84.0	51.2	48.0	60.0	72.0	66.7
SS2	82.1	92.0	64.3	75.0	57.1	72.7	89.3	73.5
SS3	86.2	89.3	37.9	73.3	24.1	63.6	62.1	81.8
PAS	77.3	98.1	72.7	98.0	90.9	85.7	87.9	95.1
WAT	95.5	100.0	81.8	100.0	100.0	95.7	95.5	100.0
NVW	53.9	87.5	84.6	73.3	46.2	100.0	61.5	100.0
URB	100.0	100.0	96.3	100.0	100.0	100.0	100.0	100.0
BUR	100.0	87.5	92.9	100.0	50.0	63.6	92.9	76.5
OCA	82.8		74.0		70.7		83.7	
OKC	0.807		0.707		0.665		0.816	

Note: MLC, CTA, MLP and OBC represent four selected classification algorithms – maximum likelihood classification, classification tree analysis, multi-layer perceptron trained by back propagation algorithm and object-based classification. UA and PA represent user's accuracy (%) and producer's accuracy (%); OCA and OKC represent overall classification accuracy (%) and overall kappa coefficient.

5.2 *Selection of a suitable classification algorithm for land-cover classification*

Nonparametric classification algorithms have some advantages over traditional classification algorithms in data requirement, but nonparametric algorithms often require the determination of many parameters, which is often time consuming and challenging to optimize. The lack of clear, standardized guidelines for the determination of the parameters requires experimentation by the analyst to identify suitable, optimized

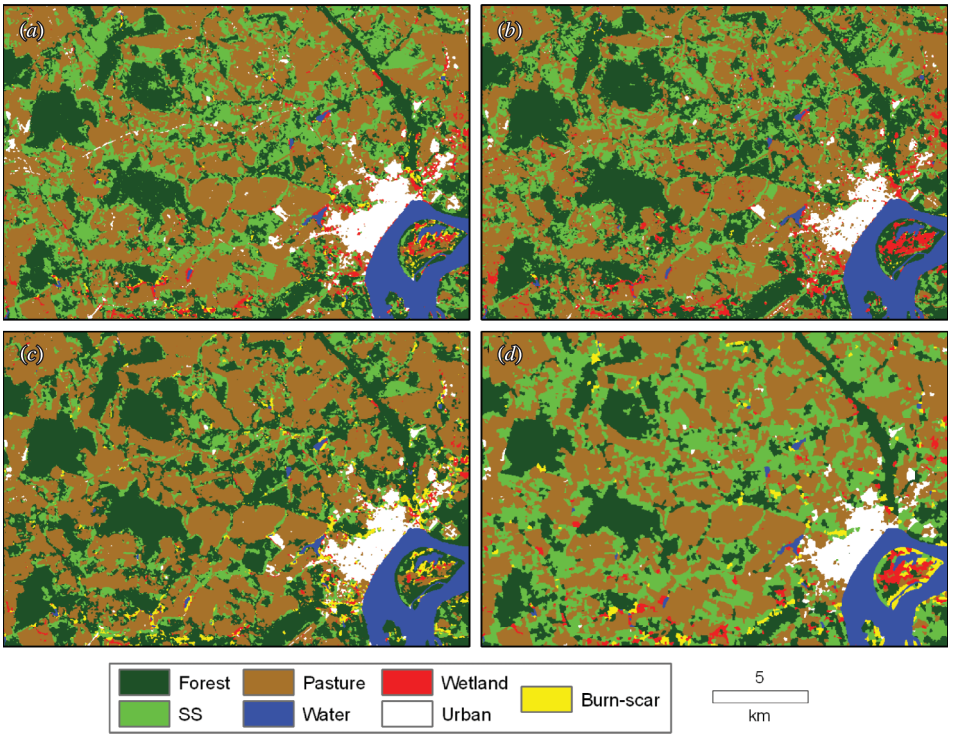

Figure 4. Comparison of classification results developed from different classification methods based on the combination of spectral bands, two vegetation indices and two textural images: (*a*) maximum likelihood classification, (*b*) regression-tree classification, (*c*) neural network and (*d*) object-based classification. (In order to clearly show the land-cover distribution, three forest classes and three SS classes were merged as forest and SS in this figure.)

parameters. For example, MLP requires much time during the training process and requires lengthy trials for identifying such parameters as learning rate, number of iterations and momentum factor. In OBC, much time is required in the development of a suitable segmentation image and often requires intensive trials in order to identify suitable parameters. One advantage of this method is that the salt-and-pepper effect can be considerably reduced, compared with the per-pixel-based classification methods. One disadvantage of this method is that the classification accuracies of some land covers may be improved, but others may be reduced, depending on the complexity of land covers under investigation and segment size. CTA requires much less time for image classification compared with MLP and OBC, and the ratio split type is often regarded better than entropy and Gini types. Comparing the nonparametric algorithms, MLC may be the most common, is often less time consuming and is recommended in this research.

6. Conclusions

This research has investigated the use of textural images and vegetation indices in land-cover classification in the moist tropical region of the Brazilian Amazon and explored their roles in improving vegetation classification performance, as well as

different classification algorithms. The results indicated that combination of vegetation indices as extra bands into Landsat TM multi-spectral bands has a limited role, but the combination of textural images was valuable for improving vegetation classification accuracy. If both vegetation indices and textural images were combined with TM multi-spectral bands, OCA can be improved by 5.6% and OKC by 6.25%. Comparison of the different classification algorithms indicated that CTA and MLP have a poor classification performance in this research, but OBC improved primary forest and pasture classification accuracies. This research indicates that use of textural images or use of OBC are especially valuable for improving the vegetation classes, such as UPF and LIF, that have complex stand structures and relatively large patch sizes. This research is valuable for guiding the selection of remote-sensing variables and classification algorithms for vegetation classification in moist tropical regions.

Acknowledgements

The authors thank the National Institute of Child Health and Human Development at NIH (grant #R01 HD035811) and the National Science Foundation (grant #BCS 0850615) for support of this research. The authors also thank Anthony Cak for help in field data collection.

References

Adams, J.B., Sabol, D.E., Kapos, V., Filho, R.A., Roberts, D.A., Smith, M.O. and Gillespie, A.R., 1995, Classification of multispectral images based on fractions of endmembers: application to land-cover change in the Brazilian Amazon. *Remote Sensing of Environment*, **52**, pp. 137–154.

Ali, S.S., Dare, P.M. and Jones, S.D., 2009, A comparison of pixel- and object-level data fusion using Lidar and high-resolution imagery for enhanced classification. In *Innovations in Remote Sensing and Photogrammetry*, S. Jones and K. Reinke (Eds.), pp. 3–17 (Berlin: Springer-Verlag).

Augusteijn, M.F., Clemens, L.E. and Shaw, K.A., 1995, Performance evaluation of texture measures for ground cover identification in satellite images by means of a neural network classifier. *IEEE Transactions on Geoscience and Remote Sensing*, **33**, pp. 616–625.

Bannari, A., Morin, D. and Bonn, E., 1995, A review of vegetation indices. *Remote Sensing Reviews*, **13**, pp. 95–120.

Bischof, H., Schneider, W. and Pinz, A.J., 1992, Multispectral classification of Landsat images using neural networks. *IEEE Transactions on Geoscience and Remote Sensing*, **30**, pp. 482–489.

Blaschke, T., 2010, Object based image analysis for remote sensing. *ISPRS Journal of Photogrammetry and Remote Sensing*, **65**, pp. 2–16.

Brondízio, E.S., Moran, E.F., Mausel, P. and Wu, Y., 1996, Land cover in the Amazon estuary: linking of the Thematic Mapper with botanical and historical data. *Photogrammetric Engineering and Remote Sensing*, **62**, pp. 921–929.

Bruzzone, L., Conese, C., Maselli, F. and Roli, F., 1997, Multisource classification of complex rural areas by statistical and neural-network approaches. *Photogrammetric Engineering and Remote Sensing*, **63**, pp. 523–533.

Butusov, O.B., 2003, Textural classification of forest types from Landsat 7 imagery. *Mapping Sciences and Remote Sensing*, **40**, pp. 91–104.

Castro, K.L., Sanchez-Azofeifa, G.A. and Rivard, B., 2003, Monitoring secondary tropical forests using space-borne data: implications for Central America. *International Journal of Remote Sensing*, **24**, pp. 1853–1894.

Chander, G., Markham, B.L. and Helder, D.L., 2009, Summary of current radiometric calibration coefficients for Landsat MSS, TM, ETM+, and EO-1 ALI sensors. *Remote Sensing of Environment*, **113**, pp. 893–903.

Chavez, Jr., P.S., 1996, Image-based atmospheric corrections – revisited and improved. *Photogrammetric Engineering and Remote Sensing*, **62**, pp. 1025–1036.

Chen, D., Stow, D.A. and Gong, P., 2004, Examining the effect of spatial resolution and texture window size on classification accuracy: an urban environment case. *International Journal of Remote Sensing*, **25**, pp. 2177–2192.

Congalton, R.G., 1991, A review of assessing the accuracy of classification of remotely sensed data. *Remote Sensing of Environment*, **37**, pp. 35–46.

Congalton, R.G. and Green, K., 2008, *Assessing the Accuracy of Remotely Sensed Data: Principles and Practices*, 2nd ed., p. 183 (Boca Raton, FL: CRC Press).

Ehlers, M., Klonus, S., Astrand, P.J. and Rosso, P., 2010, Multisensor image fusion for pansharpening in remote sensing. *International Journal of Image and Data Fusion*, **1**, pp. 25–45.

Foody, G.M., 2002, Status of land cover classification accuracy assessment. *Remote Sensing of Environment*, **80**, pp. 185–201.

Foody, G.M., 2004, Thematic map comparison: evaluating the statistical significance of differences in classification accuracy. *Photogrammetric Engineering and Remote Sensing*, **70**, pp. 627–633.

Foody, G.M., 2009, Classification accuracy comparison: hypothesis tests and the use of confidence intervals in evaluations of difference, equivalence and non-inferiority. *Remote Sensing of Environment*, **113**, pp. 1658–1663.

Foody, G.M., Palubinskas, G., Lucas, R.M., Curran, P.J. and Honzák, M., 1996, Identifying terrestrial carbon sinks: classification of successional stages in regenerating tropical forest from Landsat TM data. *Remote Sensing of Environment*, **55**, pp. 205–216.

Franklin, S.E. and Wulder, M.A., 2002, Remote sensing methods in medium spatial resolution satellite data land cover classification of large areas. *Progress in Physical Geography*, **26**, pp. 173–205.

Friedl, M.A. and Brodley, C.E., 1997, Decision tree classification of land cover from remotely sensed data. *Remote Sensing of Environment*, **61**, pp. 399–409.

Gong, P., 1994, Integrated analysis of spatial data from multiple sources: an overview. *Canadian Journal of Remote Sensing*, **20**, pp. 349–359.

Gong, P. and Howarth, P.J., 1992, Frequency-based contextual classification and gray-level vector reduction for land-use identification. *Photogrammetric Engineering & Remote Sensing*, **58**, pp. 423–437.

Hansen, M., Dubayah, R. and Defries, R., 1996, Classification trees: an alternative to traditional land cover classifiers. *International Journal of Remote Sensing*, **17**, pp. 1075–1081.

Haralick, R.M., Shanmugam, K. and Dinstein, I., 1973, Textural features for image classification. *IEEE Transactions on Systems, Man, and Cybernetics*, **SMC-3**, pp. 610–620.

Harris, P.M. and Ventura, S.J., 1995, The integration of geographic data with remotely sensed imagery to improve classification in an urban area. *Photogrammetric Engineering and Remote Sensing*, **61**, pp. 993–998.

Hill, R.A. and Foody, G.M., 1994, Separability of tropical rain-forest types in the Tambopata-Candamo reserved zone, Peru. *International Journal of Remote Sensing*, **15**, pp. 2687–2693.

Hodgson, M.E., Jensen, J.R., Tullis, J.A., Riordan, K.D. and Archer, C.M., 2003, Synergistic use Lidar and color aerial photography for mapping urban parcel imperviousness. *Photogrammetric Engineering and Remote Sensing*, **69**, pp. 973–980.

Jensen, J.R. 2004, *Introductory Digital Image Processing: A Remote Sensing Perspective*, 3rd ed., p. 526 (Upper Saddle River, NJ: Pearson Prentice Hall).

Kanellopoulos, I. and Wilkinson, G.G., 1997, Strategies and best practice for neural network image classification. *International Journal of Remote Sensing*, **18**, pp. 711–725.

KASHYAP, R.L., CHELLAPPA, R. and KHOTANZAD, A., 1982, Texture classification using features derived from random field models. *Pattern Recognition Letters*, **1**, pp. 43–50.

KUROSU, T., YOKOYAMA, S. and CHIBA, K., 2001, Land use classification with textural analysis and the aggregation technique using multi-temporal JERS-1 L-band SAR images. *International Journal of Remote Sensing*, **22**, pp. 595–613.

LANDGREBE, D.A., 2003, *Signal Theory Methods in Multispectral Remote Sensing*, p. 508 (Hoboken, NJ: John Wiley & Sons).

LI, D., 2010, Remotely sensed images and GIS data fusion for automatic change detection. *International Journal of Image and Data Fusion*, **1**, pp. 99–108.

LILLESAND, T.M. and KIEFER, R.W., 2000, *Remote Sensing and Image Interpretation*, 4th ed., p. 724 (New York: John Wiley & Sons).

LU, D., 2005a, Integration of vegetation inventory data and Landsat TM image for vegetation classification in the western Brazilian Amazon. *Forest Ecology and Management*, **213**, pp. 369–383.

LU, D., 2005b, Aboveground biomass estimation using Landsat TM data in the Brazilian Amazon. *International Journal of Remote Sensing*, **26**, pp. 2509–2525.

LU, D., BATISTELLA, M. and MORAN, E., 2007, Land cover classification in the Brazilian Amazon with the integration of Landsat ETM+ and RADARSAT data. *International Journal of Remote Sensing*, **28**, pp. 5447–5459.

LU, D., BATISTELLA, M., MORAN, E. and DE MIRANDA, E.E., 2008, A comparative study of Landsat TM and SPOT HRG images for vegetation classification in the Brazilian Amazon. *Photogrammetric Engineering and Remote Sensing*, **70**, pp. 311–321.

LU, D., HETRICK, S. and MORAN, E., 2010, Land cover classification in a complex urban-rural landscape with Quickbird imagery. *Photogrammetric Engineering and Remote Sensing*, **76**, pp. 1159–1168.

LU, D., MAUSEL, P., BATISTELLA, M. and MORAN, E., 2004a, Comparison of land-cover classification methods in the Brazilian Amazon basin. *Photogrammetric Engineering and Remote Sensing*, **70**, pp. 723–731.

LU, D., MAUSEL, P., BRONDÍZIO, E.S. and MORAN, E., 2002, Assessment of atmospheric correction methods for Landsat TM data applicable to Amazon basin LBA research. *International Journal of Remote Sensing*, **23**, pp. 2651–2671.

LU, D., MAUSEL, P., BRONDÍZIO, E.S. and MORAN, E., 2004b, Relationships between forest stand parameters and Landsat Thematic Mapper spectral responses in the Brazilian Amazon Basin. *Forest Ecology and Management*, **198**, pp. 149–167.

LU, D., MORAN, E. and BATISTELLA, M., 2003, Linear mixture model applied to Amazonian vegetation classification. *Remote Sensing of Environment*, **87**, pp. 456–469.

LU, D. and WENG, Q., 2007, A survey of image classification methods and techniques for improving classification performance. *International Journal of Remote Sensing*, **28**, pp. 823–870.

LUCAS, R.M., HONZÁK, M., CURRAN, P.J., FOODY, G.M., MILNE, R., BROWN, T. and AMARAL, S., 2000, The regeneration of tropical forests within the Legal Amazon. *International Journal of Remote Sensing*, **21**, pp. 2855–2881.

LUCAS, R.M., HONZÁK, M., DO AMARAL, I., CURRAN, P.J. and FOODY, G.M., 2002, Forest regeneration on abandoned clearances in central Amazonia. *International Journal of Remote Sensing*, **23**, pp. 965–988.

MARCEAU, D.J., HOWARTH, P.J., DUBOIS, J.M. and GRATTON, D.J., 1990, Evaluation of the grey-level co-occurrence matrix method for land-cover classification using SPOT imagery. *IEEE Transactions on Geoscience and Remote Sensing*, **28**, pp. 513–519.

MAUSEL, P., WU, Y., LI, Y., MORAN, E. and BRONDÍZIO, E., 1993, Spectral identification of succession stages following deforestation in Amazonia. *Geocarto International*, **8**, pp. 11–20.

Mausel, P.W., Kramber, W.J. and Lee, J.K., 1990, Optimum band selection for supervised classification of multispectral data. *Photogrammetric Engineering and Remote Sensing*, **56**, pp. 55–60.

McDonald, A.J., Gemmell, F.M. and Lewis, P.E., 1998, Investigation of the utility of spectral vegetation indices for determining information on coniferous forests. *Remote Sensing of Environment*, **66**, pp. 250–272.

Moran, E.F., 1981, *Developing the Amazon* (Bloomington, IN: Indiana University Press).

Moran, E.F. and Brondízio, E.S., 1998, Land-use change after deforestation. In *Amazônia, People and Pixels: Linking Remote Sensing and Social Science*, D. Liverman, E.F. Moran, R.R. Rindfuss and P.C. Stern (Eds.), pp. 94–120 (Washington, DC: National Academy Press).

Moran, E.F., Brondízio, E.S. and Mausel, P., 1994a, Secondary succession. *Research and Exploration*, **10**, pp. 458–476.

Moran, E.F., Brondízio, E.S., Mausel, P. and Wu, Y., 1994b, Integrating Amazonian vegetation, land use, and satellite data. *Bioscience*, **44**, pp. 329–338.

Narasimha Rao, P.V., Sesha Sai, M.V.R., Sreenivas, K., Krishna Rao, M.V., Rao, B.R.M., Dwivedi, R.S. and Venkataratnam, L., 2002, Textural analysis of IRS-1D panchromatic data for land cover classification. *International Journal of Remote Sensing*, **23**, pp. 3327–3345.

Paola, J.D. and Schowengerdt, R.A., 1995, A review and analysis of back propagation neural networks for classification of remotely sensed multi-spectral imagery. *International Journal of Remote Sensing*, **16**, pp. 3033–3058.

Podest, E. and Saatchi, S., 2002, Application of multiscale texture in classifying JERS-1 radar data over tropical vegetation. *International Journal of Remote Sensing*, **23**, pp. 1487–1506.

Pohl, C. and Van Genderen, J.L., 1998, Multisensor image fusion in remote sensing: concepts, methods, and applications. *International Journal of Remote Sensing*, **19**, pp. 823–854.

Richards, J.A. and Jia, X., 1999, *Remote Sensing Digital Image Analysis: An Introduction*, 3rd ed., p. 363 (Berlin: Springer-Verlag).

Rignot, E., Salas, W.A. and Skole, D.L., 1997, Mapping deforestation and secondary growth in Rondônia, Brazil using imaging Radar and Thematic Mapper data. *Remote Sensing of Environment*, **59**, pp. 167–176.

Roberts, D.A., Batista, G.T., Pereira, J.L.G., Waller, E.K. and Nelson, B.W., 1998, Change identification using multitemporal spectral mixture analysis: applications in eastern Amazônia. In *Remote Sensing Change Detection: Environmental Monitoring Methods and Applications*, R.S. Lunetta and C.D. Elvidge (Eds.), pp. 137–161 (Ann Arbor, MI: Ann Arbor Press).

Roberts, D.A., Numata, I., Holmes, K., Batista, G., Krug, T., Monteiro, A., Powell, B. and Chadwick, O.A., 2002, Large area mapping of land-cover change in Rondônia using multitemporal spectral mixture analysis and decision tree classifiers. *Journal of Geophysical Research*, **107**, 8073.

Rogan, J., Franklin, J., Stow, D., Miller, J., Woodcock, C. and Roberts, D., 2008, Mapping land-cover modifications over large areas: a comparison of machine learning algorithms. *Remote Sensing of Environment*, **112**, pp. 2272–2283.

Shaban, M.A. and Dikshit, O., 2001, Improvement of classification in urban areas by the use of textural features: the case study of Lucknow city, Uttar Pradesh. *International Journal of Remote Sensing*, **22**, pp. 565–593.

Shackelford, A.K. and Davis, C.H., 2003, A hierarchical fuzzy classification approach for high-resolution multispectral data over urban areas. *IEEE Transactions on Geoscience and Remote Sensing*, **41**, pp. 1920–1932.

Skole, D.L., Chomentowski, W.H., Salas, W.A. and Nobre, A.D., 1994, Physical and human dimension of deforestation in Amazonia. *BioScience*, **44**, pp. 314–328.

Smits, P.C., Dellepiane, S.G. and Schowengerdt, R.A., 1999, Quality assessment of image classification algorithms for land-cover mapping: a review and a proposal for a cost-based approach. *International Journal of Remote Sensing*, **20**, pp. 1461–1486.

Solberg, A.H.S., Taxt, T. and Jain, A.K., 1996, A Markov random field model for classification of multisource satellite imagery. *IEEE Transactions on Geoscience and Remote Sensing*, **34**, pp. 100–112.

Stefanov, W.L., Ramsey, M.S. and Christensen, P.R., 2001, Monitoring urban land cover change: an expert system approach to land cover classification of semiarid to arid urban centers. *Remote Sensing of Environment*, **77**, pp. 173–185.

Sun, W.X., Heidt, V., Gong, P. and Xu, G., 2003, Information fusion for rural land-use classification with high-resolution satellite imagery. *IEEE Transactions on Geoscience and Remote Sensing*, **41**, pp. 883–890.

Tso, B. and Mather, P.M., 2001, *Classification Methods for Remotely Sensed Data* (London, UK: Taylor & Francis).

Tucker, J.M., Brondízio, E.S. and Moran, E.F., 1998, Rates of forest regrowth in Eastern Amazônia: a comparison of Altamira and Bragantina regions, Para State, Brazil. *Interciencia*, **23**, pp. 64–73.

Vieira, I.C.G., de Almeida, A.S., Davidson, E.A., Stone, T.A., de Carvalho, C.J.R. and Guerrero, J.B., 2003, Classifying successional forests using Landsat spectral properties and ecological characteristics in eastern Amazonia. *Remote Sensing of Environment*, **87**, pp. 470–481.

Williams, J., 2001, *GIS Processing of Geocoded Satellite Data*, p. 327 (Chichester, UK: Springer and Praxis Publishing).

Wulder, M.A., Franklin, S.E., White, J.C., Linke, J. and Magnussen, S., 2006, An accuracy assessment framework for large-area land cover classification products derived from medium-resolution satellite data. *International Journal of Remote Sensing*, **27**, pp. 663–683.

Yanasse, C.C.F., Sant'Anna, S.J.S., Frery, A.C., Rennó, C.D., Soares, J.V. and Luckman, A.J., 1997, Exploratory study of the relationship between tropical forest regeneration stages and SIR-C L and C data. *Remote Sensing of Environment*, **59**, pp. 180–190.

Yu, Q., Gong, P., Clinton, N., Biging, G., Kelly, M. and Schirokauer, D., 2006, Object-based detailed vegetation classification with airborne high spatial resolution remote sensing imagery. *Photogrammetric Engineering & Remote Sensing*, **72**, pp. 799–811.

Zambon, M, Lawrence, R.,, Bunn, A. and Powell, S., 2006, Effect of alternative splitting rules on image processing using classification tree analysis. *Photogrammetric Engineering & Remote Sensing*, **72**, pp. 25–30.

Zhang, J., 2010, Multisource remote sensing data fusion: status and trends. *International Journal of Image and Data Fusion*, **1**, pp. 5–24.

Zhang, Y., Lu, D., Yang, B., Sun, C. and Sun, M., 2011, Coastal wetland vegetation classification with a Landsat Thematic Mapper image. *International Journal of Remote Sensing*, **32**, pp. 545–561.

2010

No. 10-03
Lu, D., S. Hetrick, and E. Moran 2010. Land Cover Classification in a Complex Urban-rural Landscape with QuickBird Imagery. Photogrammetric Engineering & Remote Sensing 76(10):1159-1168.

No. 10-04
Lu, D., E. Moran, S. Hetrick and G. Li. In Press. Mapping Impervious Surface Distribution with the Integration of Landsat TM and Quickbird Images in a Complex Urban-rural Frontier in Brazil. Chapter 16.

No. 10-05
Lu, D., S. Hetrick, and E. Moran. In Press. Impervious Surface Mapping with Quickbird Imagery. International Journal of Remote Sensing.

No. 10-06
Mattos, L. and A. Cau. In Press. The Clean Development Mechanism and Agroforestry Activities in the Brazilian Amazon.

No. 10-09
Lu, D., E. Moran, and S. Hetrick. In Press. Detection of Impervious Surface Change with Multitemporal Remote Sensing Data in an Urban-rural Frontier.

No. 10-10
D. Lu, S. Hetrick, E. Moran, and G. Li. In Press. Detection of Urban Expansion with Multitemporal Quickbird Images. International Journal of Remote Sensing.

No. 10-11
Muehlenbein, M.P., J.L. Hirschtick, J.Z. Bonner, and A.M. Swartz. 2010. Toward quantifying the usage costs of human immunity: Altered metabolic rates and hormone levels during acute immune activation in men. American Journal of Human Biology 22: 546-556.

No. 10-12
Muehlenbein, M.P., L.A. Martinez, A.A. Lemke, L. Ambu, S. Nathan, S. Alsito, and R. Sakong. 2010. Unhealthy travelers present challenges to sustainable primate ecotourism. Travel Medicine and Infectious Disease 8: 169-175.

No. 10-13
Tucker, C.M. 2010. Private Goods and Common Property: Pottery Production in a Honduran Lenca Community. Human Organization 69(1): 43-53.

No. 10-14
Tucker, C.M., H. Eakin, and E.J. Castellanos. 2010. Perceptions of risk and adaptation: Coffee producers, market shocks, and extreme weather in Central America and Mexico. Global Environmental Change 20: 23-32.

No. 10-15
Lu, D., S. Hetrick, E. Moran, and G. Li. 2010. Detection of Urban Expansion in an Urban-rural Landscape with Multitemporal QuickBird Images. Journal of Applied Remote Sensing 4(041880): 1-17.

No. 10-16
Mattos, L., E. Brondizio, A. Romeiro, and R. Orair. 2010. Agricultural de pequena escala e suas implicações na transição agroecológica na Amazônia Brasileira. Amazônica 2(2): 220-248.